Gelling synthesis of NiO/YSZ nanocomposite powder for solid oxide fuel cells

Hamood Al Kharusi[1], Mozhgan Svensson[2], Babak Salamatinia[1], Bahman Amini Horri[2*]

[1]*Chemical Engineering Discipline, Monash University Malaysia, Jalan Lagoon Selatan, Bandar Sunway, Selangor 47500, Malaysia*
[2]*Chemical and Process Engineering Department, University of Surrey, Guildford, Surrey, GU2 7XH, United Kingdom*

[*]Corresponding author; Tel: (+44) (0)1483 300800; E-mail: B.AminiHorri@Surrey.ac.uk)

Received: 10 August 2017, Revised: 15 August 2017 and Accepted: 06 September 2017

DOI: 10.5185/amp.2017/922
www.vbripress.com/amp

Abstract

NiO/YSZ (nickel oxide / yttria-stabilized zirconia) is the state-of-the-art anode composite for fabrication of high-temperature solid oxide fuel cells (SOFCs). In this study, nanocomposite powder of NiO/YSZ was synthesized by thermal treatment of the gel beads formed by extrusion dripping of sodium alginate solution into an aqueous solution of Ni^{+2}, Y^{+3}, and Zr^{+4}. The NiO/YSZ nanocomposite powder was prepared by calcination (thermal decomposition) of the dried beads in a muffle furnace at 400°C-600°C for 6 hours. The as prepared powders were characterised by TGA, XRD, FESEM, and TEM techniques. The TGA results of the dried beads showed that the thermal degradation begins at 135°C which is followed by a total mass loss of around 75.0% at 600°C. The morphology analysis of the sample (by FESEM and TEM images) showed a relatively uniform particle size distribution of the powder with an average particle size of 5-25 nm that was confirmed by the XRD crystal size calculations. The electrochemical performance measurement of the fabricated cell using the synthesized NiO/YSZ showed a maximum power density of 1143 mW/cm^2 at 850°C under hydrogen stream at 20 ml/min.

Keywords: Solid oxide fuel cells, gelling synthesis, NiO/YSZ, ceramic nanocomposites, SOFC anode.

Introduction

Solid oxide fuel cell (SOFC) has been recently considered as one of the promising energy conversion devices for electrical power generation due to its high conversion efficiency, fuel flexibility, and low emission [1, 2]. The advanced characteristics of the SOFCs may help to resolve the current environmental issues associated with using fossil fuels in the conventional energy conversion techniques as well as meeting the future trends for the world's energy demand [3]. However, commercialization of the SOFCs still depends on the progress in developing highly efficient nanocomposite materials for SOFC electrodes and electrolytes, improving the overall SOFC life-time under the operational red-ox cycles, and developing low-cost fabrication techniques for SOFC manufacturing [4-6].

In fabrication of SOFCs, the anode-supported cell design is one of the most commonly applied geometries due to offering a lower overall cell ohmic resistance and better electrochemical performance [7, 8]. Ni/YSZ (nickel/yttria-stabilized zirconia) cermet is the state-of-the-art material widely used for fabrication of SOFC anodes [6, 9]. An ideal SOFC anode should have a high electrocatalytic activity, adequate electrical conductivity, sufficient thermochemical stability especially for operating at multiple redox cycle conditions [9-11]. The anode powders used to fabricate the SOFCs with such performance characteristics should possess a homogeneous phase distribution of the ceramic and metallic constituents, proper morphology and particle size range, and a high active surface area [12-14].

In the recent years, various methods have been reported to obtain NiO/YSZ nanocomposite powders for SOFCs [8, 15]. For example, physical mixing [10, 16], hydrothermal synthesis [17, 18], combustion technique [19-21], co-precipitation [11, 22], sol-gel method [23, 24], spray pyrolysis [25-27], microwave assisted technique [13, 28] are some of the frequently applied methods for preparation of NiO/YSZ powders in literatures. However, many of these methods are usually associated with complex steps and costly processes which may not be ideal for commercial applications [29]. Therefore, developing simple single-step, cost-effective, efficient, and environmental-friendly processes for the preparation of high quality ceramic nanocomposite powders is of great interests not only by for research purposes but also for the SOFC industrial communities [29-32].

We have recently developed a novel green method for synthesizing gadolinium doped ceria ($Ce_{0.8}Gd_{0.2}O_{1.90}$)

using ionic-gelation method [33]. Here in this paper, we report for the first time the application ionic-gelation method mediated by alginate route as an efficient, environmentally-benign, and low-cost synthesis method for NiO/YSZ nanocomposite powder.

In this study, sodium alginate as the jelling template was applied to synthesize high purity NiO/YSZ (8 mol%, $Zr_{0.92}Y_{0.08}O_{1.96}$) nanocomposite powder. The influence of calcination temperature on the purity and particle size of the synthesized NiO/YSZ nanocomposite powders was investigated. The physiochemical properties of the synthesized powders were studied using thermogravimetric analysis (TGA), X-ray diffraction (XRD), Field Emission Scanning Electron Microscopy (FESEM), Energy-dispersive x-ray spectroscopy (EDX), Fourier transform infrared spectroscopy (FTIR) and Nitrogen adsorption-desorption (BET). The cell electrochemical performance was measured by fabricating a single cell using the synthesized anode powder. The proposed method by this study could be used as an alternative method for synthesizing SOFC anode nanocomposite using renewable green resources. This study could be helpful to provide a better understanding of the synthesis and calcination of the composite metal oxides using ionic gelling method.

Experimental

Materials

Manugel GHB sodium alginate powder ($(C_6H_7NaO_6)_n$, MW: 264 kDa) with an M/G ratio of 0.59 (BioPolymer, UK) was used as the jelling template. Also, Zirconium(IV) oxychloride octahydrate ($ZrOCl_2.8H_2O$, 99.5%), Yttrium(III) nitrate hexahydrate ($Y(NO_3)_3{\cdot}6H_2O$, 99.8%), and Nickel(II) nitrate hexahydrate ($Ni(NO_3)_2{\cdot}6H_2O$, 99.9%) all from Sigma Aldrich., USA were used as the cationic solution source in this work. To fabricate the single cells, commercial grade of yttria stabilized zirconium(IV) oxide, YSZ (ZrO_2,Y_2O_3, 99.9%) as the electrolyte powders and lanthanum strontium manganite ($La_{0.8}Sr_{0.2}MnO_{3-\delta}$, LSM-20, 99^{+}%) as the cathode active powder were obtained from Sigma-Aldrich along with reagent solvents including n-propanol, isopropanol, and ethylene glycol.

NiO/YSZ synthesis

In this study, the gelling beads were prepared by extrusion dripping of sodium alginate solution (2±0.1 wt.%) into an aqueous solution containing Ni^{+2}, Y^{+3}, and Zr^{+4} cations (80±1 g/L). The cationic solution was prepared by dissolving the given amount of the corresponding metallic nitrate precursors (listed in the Material section) in order to result in a NiO/YSZ mixture (50/50 by wt.) for a typical 8 mol% YSZ. The beads were collected, washed, and then dried in an oven at 50°C for 24 h. The NiO/YSZ nanocomposite powder was prepared by calcination (thermal decomposition) of the as prepared dried beads in a muffle furnace at 400-600°C for 6 h.

Cell fabrication

The experimental procedure used in this work to fabricate the SOFC anode supported single cells has been explained in details elsewhere [7]. In a typical experiment, the as prepared NiO/YSZ nanocomposite powder was used to fabricate the supporting anodes (disc shape, 10mm diameter and 0.8mm thickness) by die pressing method followed by pre-sintering at 1000°C for 4 h. Then a thin layer of electrolyte (20±5μ) was integrated over the supporting anodes by a spin coater (VTC-200P, KGC resources, rotating at 900 rpm for 1 min) using a suspension of the commercial YSZ in n-propanol (50 g/L). After sintering the bi-layers at 1350°C (4 h), the cathode layer (60±20μ) was brush painted over the specimens using a suspension (300 g/L) containing LSM/YSZ mixture (50/50 wt.%) in isopropanol (75 wt.%) and ethylene glycol (25 wt.%) mixture. The single cells were then co-sintered at 1150 for 3 h that was followed by reduction in a tube furnace at 800°C for 2 h using humidified hydrogen stream.

Material characterization and cell performance measurement

Thermogravimetric spectra obtained by a TGA analyzer (Q50, USA) in air for a temperatures ranging from 25 °C to 700 °C with a ramp rate of 5 °C/min. An XRD diffractometer (XRD, D8 Discover Bruker., Germany) was used to provide X-ray diffraction patterns with CuKα1 irradiation (λ=1.54060 Å) in the 2θ range between 20° and 85° and a scanning rate of 0.02°/s at 40 kV and 40 mA. The morphology of the as prepared NiO/YSZ nanocomposite powders were observed by the micrograph images obtained from a field emission scanning electron microscope (FESEM, SU8010 Hitachi, Japan). An energy-dispersive x-ray (Oxford Horiba Inca XMax50 EDX) analysis attached to the FESEM was used to obtain the elemental analysis of the prepared samples. The FTIR spectra of the calcined and the dried powders were obtained by a Fourier transform infrared spectroscopy analyzer (FTIR, NICOLET 1810., USA) over the wavenumber range of 700–4000 cm−1. The electrochemical performance of the single cells was measured in a tube furnace (at 850°C) using a DC electronic load (8500, B&K Precision, USA) interfaced with a computer and a stop I-V voltage set at 0.2 V. A humidified hydrogen gas was streamed over the anode side while the cathode was allowed to have a free contact with air.

Results and discussion

Fig. 1a shows the TGA spectra of the dried beads before calcination. As it is shown in this figure, three weight-loss stages could be observed in this figure. The first stage (starting about 30℃, with reaching a maximum evaporation rate at around 80℃, and ending at 135°C) is due to losing the moisture content by the beads. This is because of the presence of the hydrophilic groups in the

molecular structure of alginate that causes the dried bead to act as a natural hydrogel by absorbing a high level of water content from the surrounding atmosphere [34].

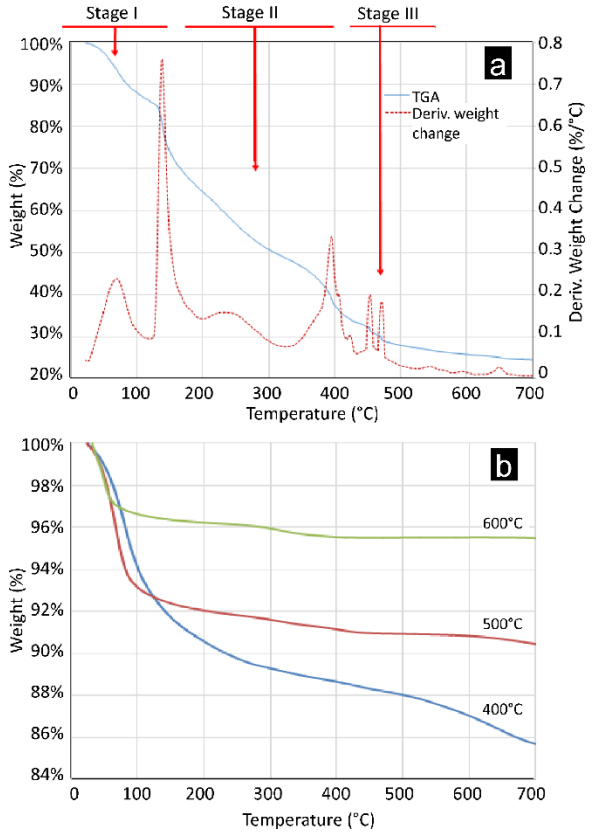

Fig. 1 TGA spectra of (**a**) dried Ni/Zr/Y/alginate beads before calcination; and (**b**) the as prepared NiO/YSZ after calcination (at 400, 500, and 600°C for 6h)

The second stage could be due to decomposition of the Alginate macromolecule into smaller molecules followed by thermal oxidation of the resulting hydrocarbons with formation of metal carbonates, CO2, CO, and H2O which is an endothermic process [35, 36]. The metal oxides composite powder (NiO/YSZ) is formed finally at stage III by degradation of the resulting products of the thermal decomposition of the alginate bead. This stage is started at around 330°C with achieving a high rate of thermal degradation around 400°C and a couple of smaller degradation peaks at about 460°C and 480°C by showing an insignificant weight-loss above 500°C. Analyzing the data by this figure, shows that the dried Ni/Zr/Y-alginate beads lose almost 75% of their initial weight below 600℃ indicating the organic polymer can be entirely removed from the dried samples by choosing the calcination temperature at or below 600℃.

Fig. 1b shows the TGA curves of the as prepared NiO/YSZ powders by calcination of the dried beads at 400, 500 and 600℃ for 6 h. The observed trends show a common dehydration (loosing moisture content) process for all samples at a temperature below 130℃ along with combination of a more noticeable decomposition process for the samples calcined at 400 °C and 500℃. Data analysis of the TGA curves shows that the weight-loss of about 4.5%, 9.5, and 14.3% are associated with the samples calcined at 600, 500, and 400°C respectively. The main reason of the large weight-loss associated with the samples calcined at lower temperatures could be due to incomplete degradation of the alginate products below 500°C [34, 36]. Although, increasing the calcination temperature may help to get a fully decomposed alginate product, however this could result in formation of bigger particle sizes and less surface areas due to agglomeration of particles (as it is described in XRD and FESEM results).

Fig. 2 shows the XRD spectra of the as-prepared NiO/YSZ nanocomposite powders. As indexed on **Fig. 2**, the XRD diffraction patterns of the synthesized powders (especially at 500 and 600°C) exhibit the main peaks of cubic-fluorite YSZ (represented by the reflection planes 111, 200, 220, and 311 corresponding to JCPDS file 30-1468 for YSZ-8 mol%, [37]) and the face-centered cubic crystals of NiO (by the reflection planes 111, 200, 220, and 311 corresponding to JCPDS 4-0835, [38]) which confirm the presence of homogeneous phase of both constituents. No characteristic peaks from other phases were detected that indicates the high purity of the synthesized product.

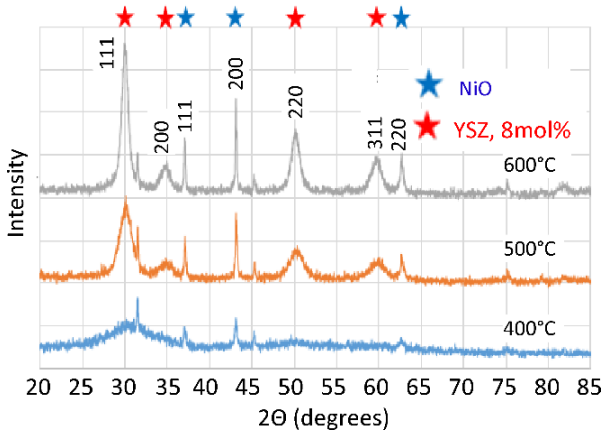

Fig. 2. XRD pattern of the as prepared NiO/YSZ powders calcined at 400, 500, and 600°C for 6h.

The XRD pattern of the sample prepared at lower temperature (400°C) does not show the main peaks of both phases indicating incomplete degradation of the alginate beads which is clearly shown by the TGA analysis as well (**Fig 1b**). In addition, as a trend it could be observed that by increasing the calcination temperature, the peaks become sharper with showing a higher intensity that indicates formation of bigger crystals possibly due to agglomeration [39]. The application of Scherrer's equation ($D=0.9\lambda/\beta\cos\theta$, where D, λ, and β are the crystallite size in nm, the wavelength in nm, and the full width at half maximum, respectively [33]) resulted in obtaining 4.90, 13.43, and 25.64 nm as the estimated crystal size of the samples calcined at 400, 500, and 600℃ respectively, which are in a good agreement with the results of the morphological analysis.
Fig. 3a shows the FTIR spectrum of the dried beads before calcination. The broad absorption peak observed at

3194.6cm^{-1} could be assigned to the hydroxyl stretching vibrations due to the presence of the OH functional group in alginate structure [40].

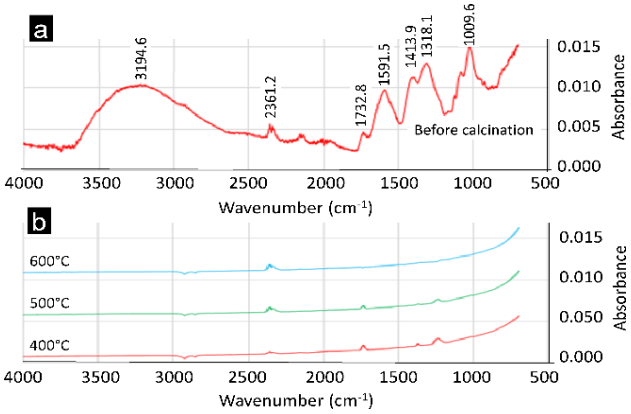

Fig. 3. FTIR spectra of (**a**) the dried Ni/Zr/Y/alginate beads before calcination; and (**b**) the as prepared NiO/YSZ after calcination (at 400, 500, and 600°C for 6h).

The vibration bands with peaks at 1009.6cm^{-1} and 1318.1cm^{-1} can be attributed to C-O-C and C–O stretching, respectively [41, 42]. The other three peaks observed at 1732.8 cm-1, 1591.5cm-1, and 1413.9 cm-1 could represent the COO^{-}, $(COO)_{asym}$, and $(COO)_{sym}$ functional groups respectively, within the alginate polymer structure [42, 43]. In addition, the small peak observed at 2360cm^{-1} could normally because of the presence of the environmental CO2 gas in the porous structure of the beads.

As shown in **Fig. 3b**, all three samples showed a complete disappearance of the hydroxyl functional group, however for the samples calcined at 400℃ and 500℃ there could be observed some detectible carboxylic functional groups at some extents. Similar to the dried beads, all the as prepared NiO/YSZ powders show the presence of small amount of CO2 that may be remained in the powders due to applied thermal treatment during the calcination process.

The particle size and morphology of the synthesized powders were examined by FESEM and TEM analysis. The FESEM image represented by **Fig. 4a, b, and c** show the morphology of NiO/YSZ nanocomposite powder synthesized by calcination of the alginate beads at 400°C, 500°C, and 600°C, respectively. These high-magnification FESEM images could show the formation of the segregated bunches of semi-spherical and semi-uniform particles that reveals the production of a homogenous distribution of their constituents. Comparing the particle sizes observed by these figures could show a trend whereas by increasing the calcination temperature, the particle sizes of the as prepared NiO/YSZ powders have been increased. The similar trend was also obtained through the application of Scherrer's equation (in XRD discussion) to get the crystallite size of the powders. This trend could be explained as a result of the tendency of smaller particles to be connected together in order to form larger particles during thermal treatment of metal oxides [9]. Another reason may be the agglomeration of particles that mainly occurs at higher temperature during the sintering processes of ceramic powders that could be because of a range of reasons such as uncontrolled buildup, bridging, or lumping phenomena [33]. The morphology and structure details of the as-prepared NiO/YSZ samples were further analyzed by TEM imaging. **Fig. 4d** represents a typical TEM image of the sample prepared at 600°C that shows a consistent morphological characteristic with that of observed by FESEM imaging. The TEM image could also give a better estimation of the particle size compared to XRD as it is much less susceptible to the particles properties such as strain and size distribution [44]. Analyzing the TEM image (**Fig. 4d**) indicates that semispherical NiO/YSZ nanoparticles with average crystallite sizes of 25 nm have been formed by calcination of the alginate sample at 600°C for 6h that confirms the estimated particle size analysis through XRD (Scherrer's equation). Furthermore, it could be seen that the majority of the particles formed by this method are monodispersed grains with minimum agglomerations.

Fig. 4e shows the FESEM image of the cross-sectional area of the anode supporting layer after sintering (before reduction). This figure indicates a high yield of grain growth and a good uniformity of the product could be obtained by sintering the as-prepared NiO/YSZ powder. The images also shows that a microscopic porous structure have been formed for the anode layer which is desirable for SOFC fabrication. The average grain size observed by analyzing Fig. 4e is around 1-2 micron that indicates the presence of a high surface area and the formation of more active reaction sites for the SOFC anode.

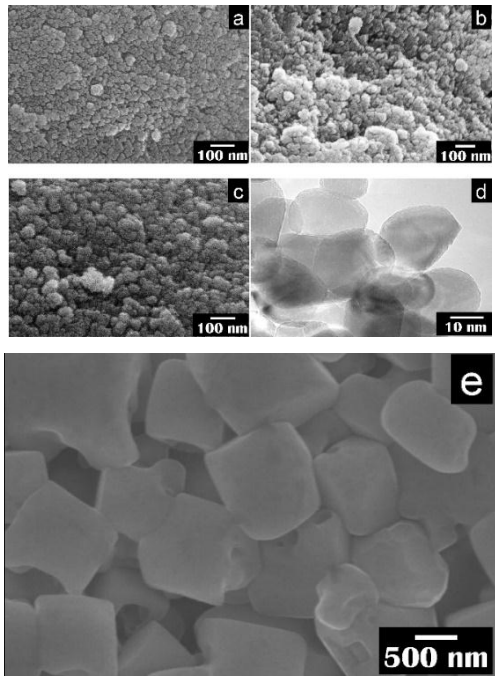

Fig. 4. FESEM image of the as prepared NiO/YSZ calcined at (**a**) 400°C, (**b**) 500°C, (**c**) 600°C, along with (**d**) TEM image the as prepared NiO/YSZ calcined at 600°C, and (**e**) the NiO/YSZ sintered anode at 1350°C (before reduction).

Table 1 represents a typical EDX elemental analysis obtained for the as prepared NiO/YSZ powder (the sample calcined at 650 °C) which confirms the presence of nickel, zirconium, yttrium, and oxygen atoms in synthesized nanocomposite. The theoretical values for the atomic mole percentage of the presenting elements (Ni, Zr, Y, and O) were calculated for the targeting product which is NiO/YSZ-8 (50:50 wt.%). As it is shown by the table, there is a small percentage error between the theoretical and the experimental values of the atomic mole percentage for the presenting elements indicating a high purity of the synthesized nanocomposite.

Table 1. Atomic compositing the as prepared NiO/YSZ at 600°C for 6h, measured at 20 kV.

Elements	Experimental Mole %	Theoretical Mole %
Ni Kα	27.05	26.34
Zr Lα	12.34	13.77
Y Lα	1.99	2.40
O Kα	56.18	57.49
C, Pt, Na, Al	2.24	0.00

The electrochemical performance of the fabricated cell using the as prepared NiO/YSZ (calcined at 600°c) was measured after reduction of the NiO in the anode into Ni using a humidified hydrogen stream (at 800°C). **Fig. 5** shows the electrochemical performance characteristic curves of the fabricated single cell by representing the operational voltage and power density of the cell vs. its current density. Before starting the performance measurements, the cell was activated at a higher hydrogen flow rate (around 40 ml/min). The fuel flow rate was gradually decreased to around 20 ml/min, while the OCV (open circuit voltage) was kept at an achieved maximum value.

According to **Fig. 5** the maximum power density obtained from the cell fabricated using the synthesized powders of this work is around 1,143 mW/cm^2 at 2100 mA/cm^2. This high electrochemical performance can verify the high quality of the NiO/YSZ nanocomposite

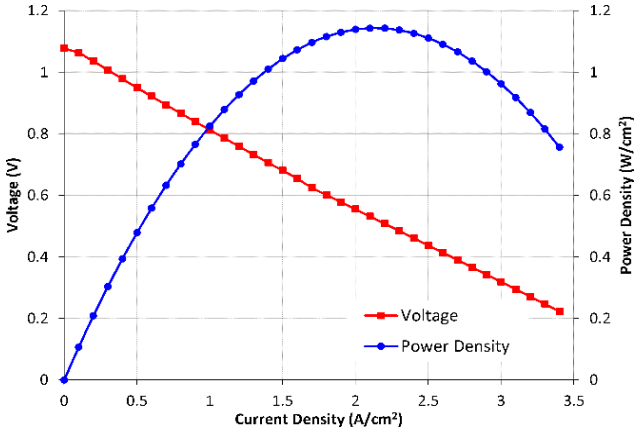

Fig. 5. Electrochemical performance of the anode-supported cell measured at 850°C under flowing a humidified hydrogen gas flowing at 20 ml/min.

powders synthesized in this work. Obtaining a high electrochemical performance in a cell could be an indication of achieving an improved electrocatalytic activity which is mainly governed by presence of more active triple boundary phase (TBP) sites and uniformly distributed Ni phase in the anode structure [10, 45].

Conclusion

In summary, NiO/YSZ nanocomposite powders have been successfully prepapred by a facile gelling synthesis method. The as-prepared NiO/YSZ samples had a particle size ranging from 5 to 25 nm. It was found that the calcination temperature could effectively change the crystalline structure and the particle size of the synthesized nanocomposite. The SOFC supporting anode fabricated by sintering of the as-prepared NiO/YSZ samples showed a high yield of grain growth and a good uniformity. A high-power density (around 1,143 mW/cm^2 at 2100 mA/cm^2) was obtained from the electrochemical performance measurement of a typical single cell in this work that indicates synthesizing a high quality anode powder (NiO/YSZ nanocomposite) by this study.

Acknowledgements

This work was a joint research study supported by a final year research project at Monash University (Malaysia) and a postdoc research project at University of Surrey. The authors are thankful for the support received from Professor Bob Slade (Department of Chemistry, University of Surrey) for some supplementary analytical tests for this study.

Author's contributions

Conceived the plan: bah; Performed the expeirments: hak, ms; Data analysis: hak, bs, bah; Wrote the paper: ms, bah. Authors have no competing financial interests.

References

1. Jacobson, A.J., *Chemistry of Materials*, **2009**, 22, 660. **DOI:** 10.1021/cm902640j
2. Choudhury, A., Chandra, H., Arora, A., *Renew. Sust. Energy Rev.*, **2013**, 20, 430. **DOI:** 10.1016/j.rser.2012.11.031
3. Belousov, V.V., *Acc. Chem. Res.*, **2017**, 50, 273. **DOI:** 10.1021/acs.accounts.6b00473
4. Wang, S., Jiang, S.P., *Natl Sci Rev*, **2017**, 4, 163. **DOI:** 10.1093/nsr/nww099
5. Kan, W.H., Thangadurai, V., *Ionics*, **2015**, 21, 301. **DOI:** 10.1007/s11581-014-1334-6
6. Gorte, R., Vohs, J., *Current Opinion in Colloid & Interface Science*, **2009**, 14, 236. **DOI:** 10.1016/j.cocis.2009.04.006
7. Horri, B.A., Selomulya, C., Wang, H., *Int. J. Hydrogen Energy*, **2012**, 37, 19045. **DOI:** 10.1016/j.ijhydene.2012.10.005
8. Shri Prakash, B., Senthil Kumar, S., Aruna, S.T., *Renew. Sust. Energy Rev.*, **2014**, 36, 149. **DOI:** 10.1016/j.rser.2014.04.043
9. Horri, B.A., Selomulya, C., Wang, H., *Int. J. Hydrogen Energy*, **2012**, 37, 15311. **DOI:** 10.1016/j.ijhydene.2012.07.108
10. Martins, R.F., Brant, M.C., Domingues, R.Z., Paniago, R.M., Sapag, K., Matencio, T., *Mater. Res. Bull.*, **2009**, 44, 451. **DOI:** 10.1016/j.materresbull.2008.04.017
11. Xi, X., Kondo, A., Naito, M., *J. Alloys Compd.*, **2016**, 688, 1047. **DOI:** 10.1016/j.jallcom.2016.07.151

12. Kim, S.-D., Moon, H., Hyun, S.-H., Moon, J., Kim, J., Lee, H.-W., *Solid State Ionics*, **2007**, 178, 1304. **DOI:** 10.1016/j.ssi.2007.06.014
13. Singh, K.L., Kumar, A., Singh, A.P., Sekhon, S.S., *Bull. Mater. Sci.*, **2008**, 31, 655. **DOI:** 10.1007/s12034-008-0104-3
14. Khan, M.S., Lee, S.-B., Song, R.-H., Lee, J.-W., Lim, T.-H., Park, S.-J., *Ceram. Int.*, **2016**, 42, 35. **DOI:** 10.1016/j.ceramint.2015.09.006
15. Lim, H.H., Sulistya, E., Wong, M.Y., Salamatinia, B., Amini Horri, B. (2017) in Mishra, A.K. (ed)Sol-gel Based Nanoceramic Materials: Preparation, Properties and Applications **DOI:** 10.1007/978-3-319-49512-5
16. Cho, H.J., Choi, G.M., *J. Power Sources*, **2008**, 176, 96. **DOI:** 10.1016/j.jpowsour.2007.09.118
17. Kim, B., Cho, K., Choi, J., Shin, D., *J. Nanosci. & Nanotechnol.*, **2015**, 15, 536. **DOI:** 10.1166/jnn.2015.8400
18. Zielke, P., Xu, Y., Kiebach, W.-R., Simonsen, S.B., Norby, P., Hendriksen, P.V., *Meeting Abstracts*, **2016**, MA2016-02, 2953. **DOI:** MA2016-02/39/2953.short
19. Singh, G., Jalandhar, D., Singh, K.L., *Renew. Energy Resour.*, **2012**, 2, 6. **DOI:** 10.18535/ijetst
20. Priyatham, T., Bauri, R., *Mater. Charact.*, **2010**, 61, 54. **DOI:** 10.1016/j.matchar.2009.10.005
21. Liang, M., Yu, B., Wen, M., Chen, J., Xu, J., Zhai, Y., *Int. J. Hydrogen Energy*, **2010**, 35, 2852. **DOI:** 10.1016/j.ijhydene.2009.05.006
22. Xi, X., Abe, H., Naito, M., *Ceram. Int.*, **2014**, 40, 16549. **DOI:** 10.1016/j.ceramint.2014.08.009
23. Keech, P.G., Trifan, D.E., Birss, V.I., *J. Electrochem. Soc.*, **2005**, 152, A645. **DOI:** 10.1149/1.1855875
24. Suciu, C., Hoffmann, A.C., Dorolti, E., Tetean, R., *Chem. Eng. J.*, **2008**, 140, 586. **DOI:** https://doi.org/10.1016/j.cej.2008.02.006
25. Yoon, Y.S., Im, J.M., Shin, D.W., *Ceram. Int.*, **2008**, 34, 873. **DOI:** http://dx.doi.org/10.1016/j.ceramint.2007.09.039
26. Lim, C.-H., Lee, K.-T., *J. Korean Ceram. Soc*,, **2014**, 51, 243.
27. Fukui, T., Ohara, S., Naito, M., Nogi, K., *Powder Technol.*, **2003**, 132, 52. **DOI:** 10.1016/S0032-5910(03)00044-5
28. Mohebbi, H., Ebadzadeh, T., Hesari, F.A., *Powder Technol.*, **2009**, 188, 183. **DOI:** 10.1016/j.powtec.2008.04.095
29. Birol, H., Rambo, C.R., Guiotoku, M., Hotza, D., *RSC Adv.*, **2013**, 3, 2873. **DOI:** 10.1039/C2RA21810K
30. Zhang, L., Lan, R., Kraft, A., Wang, M., Tao, S., *Electrochem. Commun.*, **2010**, 12, 1589. **DOI:** 10.1016/j.elecom.2010.08.038
31. Li, F., Jiang, L., Zeng, R., et al., *Int. J. Hydrogen Energy*, **2015**, 40, 12750. **DOI:** 10.1016/j.ijhydene.2015.07.104
32. Zhang, L., Li, D., Zhang, S., *Ceram. Int.*, **2017**, 43, 2859. **DOI:** 10.1016/j.ceramint.2016.10.188
33. Pezeshkpour, S., Abdullah, A.Z., Salamatinia, B., Amini Horri, B., *Ceram. Int.*, **2017**, 43, 7123. **DOI:** 10.1016/j.ceramint.2017.02.145
34. Soares, J., Santos, J., Chierice, G., Cavalheiro, E., *Eclética Química*, **2004**, 29, 57. **DOI:** 10.1590/S0100-46702004000200009
35. Mu, J., Perlmutter, D.D., *Thermochim. Acta*, **1981**, 49, 207. **DOI:** 10.1016/0040-6031(81)80175-X
36. Said, A.A., Hassan, R.M., *Polym. Degrad. Stab.*, **1993**, 39, 393. **DOI:** 10.1016/0141-3910(93)90015-B
37. Batista, R.M., Muccillo, E.N.S., *Ceram. Int.*, **2011**, 37, 1047. **DOI:** 10.1016/j.ceramint.2010.11.031
38. Amini Horri, B. PhD thesis, Monash University. Faculty of Engineering. Chemical Engineering (**2012**) **DOI:** Repository/monash:89833
39. Elshazly, E.S., Abdelal, O.A., *Int. J. Metall. Eng.*, **2012**, 1, 130. **DOI:** 10.5923.j.ijmee.20120106.07.html
40. Daemi, H., Barikani, M., *Scientia Iranica*, **2012**, 19, 2023. **DOI:** 10.1016/j.scient.2012.10.005
41. Sarker, B., Papageorgiou, D.G., Silva, R., et al., *Journal of Materials Chemistry B*, **2014**, 2, 1470. **DOI:** 10.1039/C3TB21509A
42. Mandal, B., Ray, S.K., *Carbohydr. Polym.*, **2013**, 98, 257. **DOI:** 10.1016/j.carbpol.2013.05.093
43. Papageorgiou, S.K., Kouvelos, E.P., Favvas, E.P., Sapalidis, A.A., Romanos, G.E., Katsaros, F.K., *Carbohydr. Res.*, **2010**, 345, 469. **DOI:** 10.1016/j.carres.2009.12.010
44. Danial, A.S., Saleh, M.M., Salih, S.A., Awad, M.I., *J. Power Sources*, **2015**, 293, 101. **DOI:** 10.1016/j.jpowsour.2015.05.024
45. Shearing, P.R., Gelb, J., Yi, J., Lee, W.K., Drakopolous, M., Brandon, N.P., *Electrochem. Commun.*, **2010**, 12, 1021. **DOI:** 10.1016/j.elecom.2010.05.014

